This article has been accepted for inclusion in a future issue of this journal. Content is final as presented, with the exception of pagination.

A Joint Crest Factor Reduction and Digital Predistortion for Power Amplifiers Linearization Based on Clipping-and-Bank-Filtering

Siqi Wang, Morgan Roger, *Member, IEEE*, Julien Sarrazin, *Member, IEEE*, and Caroline Lelandais-Perrault

***Abstract*— The power efficiency and the linearity of a power amplifier (PA) depend on its operating point. A high efficiency generally corresponds to poor linearity. To optimize the efficiency/linearity tradeoff, crest factor reduction (CFR) techniques are classically implemented along with digital predistortion (DPD) to control the PA operating point. Joint CFR/DPD can be realized with a single model so that the running complexity of the CFR is negligible. This article fully explores the clipping-and-bank-filtering (CABF) method for joint CFR/DPD and extends it to the multicarrier case with validation of experimental results. Compared with conventional approaches, it provides either better linearization performance or lower complexity at the same PA operating point. The study is completed with a discussion on the choice of windows in the filter bank. The proposed CABF-based joint CFR/DPD model is then experimentally evaluated on a test bench with two PAs using single-carrier and two-carrier 20-MHz long-term evolution signals as the stimulus.**

***Index Terms*— Crest factor reduction (CFR), digital predistortion (DPD), nonlinear distortion, power amplifiers (PAs), running complexity.**

I. Introduction

IN MODERN wireless telecommunication systems, power amplifiers (PA) consume the majority of power. Improving their power efficiency in transmitting data is an important concern for green communications [1]. The power efficiency of the PA is strongly correlated with its operating point [2]. When the PA operates near the saturation zone, the power efficiency approaches its maximum, but the PA is very nonlinear.

Digital predistortion (DPD) is an efficient choice to compensate for the nonlinearities and the memory effects of the PA near saturation. Basically, the DPD has the inverse characteristics of the PA and is applied upstream of the PA in a transmitter circuit [3]. Numerous DPD models based on Volterra series have been studied, such as memory polynomial (MP) [4], [5], generalized MP (GMP) [6], dynamic-deviation-reduction [7], complexity-reduced Volterra series [8], and the decomposed vector rotation-based behavioral model [9]. Block-oriented nonlinear systems have also been studied as DPD [10]–[12].

With the linearization by DPD, the main constraint on the PA operating point is the peak-to-average power ratio (PAPR) of the modulated signal, e.g., orthogonal frequency division multiplexing signals [13]. In order to avoid the PA saturation, an output backoff (OBO) at least equal to the PAPR is needed.

Numerous crest factor reduction (CFR) techniques have been studied to reduce the PAPR when DPD is used [14]–[16]. CFR is usually implemented as a correction to reduce signal peaks. It can be applied at the DPD input or the DPD output—even both—with different methods [17].

Though CFR helps to increase the PA efficiency, it deteriorates the system linearity, especially if basic hard clipping (HC) is used. The error vector magnitude (EVM) and the adjacent channel power ratio (ACPR) are often used to characterize the in-band and out-of-band errors, respectively. As the ACPR requirements are more stringent than that of EVM, the clip-and-filter (CAF) approach enables to trade off in-band errors for reduced out-of-band errors compared with HC [18]. Another approach is to implement the CFR as a parametric model, which we refer to as modeled CFR (MCFR). For instance, a polynomial soft clipping method has been proposed in [19] as CFR at the DPD input. The polynomial coefficients are estimated by minimizing the PAPR under the constraints of ACPR requirements. Because the soft clipping compresses only the signal amplitude, the EVM value can be improved at the receiver using a postcompensation method.

In [14], the MCFR is applied to the DPD output signal. If the MCFR and the DPD share the same model structure, they can be merged into a single joint CFR/DPD model whose coefficients are equal to the difference of the MCFR and the DPD coefficients. Wang *et al.* [17] compared different CFR methods by studying their impact on linearity for several OBO values, in the presence of DPD. The joint CFR/DPD model is found having a great advantage in terms of the computational burden added by the CFR. The joint CFR/DPD by a single model has the same running complexity as the DPD. This is especially interesting in the applications of coming 5G and femtocell systems because they have more stringent requirements on the complexity of the digital signal processing part since this complexity is no longer negligible to the power consumed by the PA [20], [21].

Manuscript received July 12, 2019; revised September 18, 2019 and October 30, 2019; accepted November 17, 2019. *(Corresponding author: Siqi Wang.)*

S. Wang, M. Roger, and C. Lelandais-Perrault are with GeePs, Group of Electrical Engineering, CNRS, CentraleSupélec, University of Paris-Sud, University of Paris-Saclay, Sorbonne Université, 91192 Gif-sur-Yvette, France (e-mail: siqi.wang@centralesupelec.fr; morganroger@centralesupelec.fr; caroline.lelandais-perrault@centralesupelec.fr).

J. Sarrazin is with the Laboratory of Electronics and Electromagnetism, Sorbonne Université, F-75005 Paris, France (e-mail: julien.sarrazin@sorbonne-universite.fr).

Color versions of one or more of the figures in this article are available online at http://ieeexplore.ieee.org.

Digital Object Identifier 10.1109/TMTT.2019.2956036

0018-9480 © 2019 IEEE. Personal use is permitted, but republication/redistribution requires IEEE permission.
See http://www.ieee.org/publications_standards/publications/rights/index.html for more information.

This article has been accepted for inclusion in a future issue of this journal. Content is final as presented, with the exception of pagination.

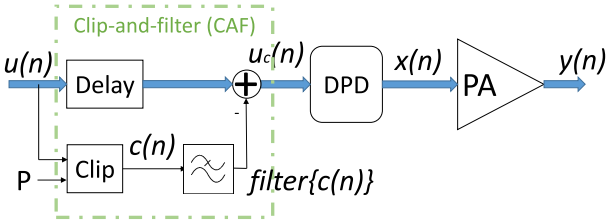

Fig. 1. Structure of CAF in front of DPD.

Regarding model coefficient estimation, the model input signal and its desired output signal are necessary. The DPD identification is usually based on the input and the output signals of the PA [22]. The MCFR coefficients can be estimated in a similar way using the stimulus and a reference correction signal. The reference correction signal has a great impact on the performance of the joint CFR/DPD model in terms of linearity.

In the literature for joint CFR/DPD structures [14], the reference correction signal is generated by clipping the predistorted signal using CAF. In [23], a clipping-and-bank-filtering (CABF) approach is proposed to improve the accuracy of the reference correction signal for single-carrier stimuli. Simulations showed promising results.

This article generalizes the CABF method to multicarrier stimulus and demonstrates its validity with experimental results. It also discusses the choice of windows for the CABF decomposition filters. The proposed method is validated on a test bench with two real PAs, first with a single carrier, then a two-carrier 20-MHz long-term evolution (LTE) signal.

This article is organized as follows. Section II recalls the conventional methods of implementing CFR and DPD. Section III presents the structure of the proposed CABF-based joint CFR/DPD, and different approaches to compute the reference correction signal for single-carrier and multicarrier stimuli are detailed. In Section IV, the experimental results are presented and discussed. Finally, the conclusion is given in Section V.

II. Conventional CFR and DPD Methods

A. Traditional CAF With DPD

CAF is one of the most used CFR algorithms. When used in conjunction with DPD, it is generally applied to the DPD input, as shown in Fig. 1, since this architecture provides better performances [17]. The clipping principle is to detect the peaks of the DPD input signal $u(n)$ with a given threshold P and to compute the corresponding correction signal

$$c(n) = \begin{cases} u(n)\left(1 - \frac{P}{|u(n)|}\right), & \text{if } |u(n)| \geq P \\ 0 & \text{otherwise.} \end{cases} \quad (1)$$

This HC introduces undesirable out-of-band frequency components. The CAF applies a filter to tradeoff out-of-band components of $c(n)$ for in-band components. The final signal is, therefore,

$$u_c(n) = u(n) - \text{filter}\{c(n)\}. \quad (2)$$

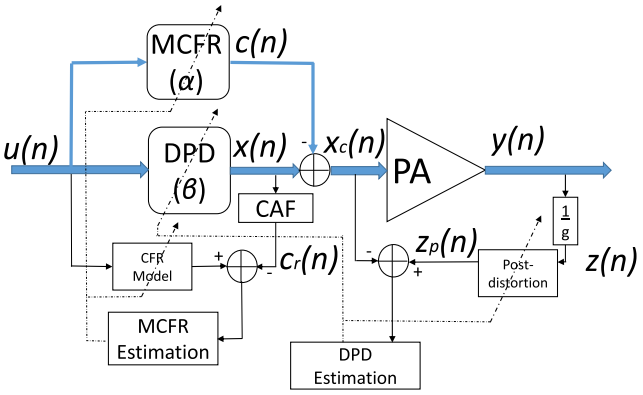

Fig. 2. Conventional joint CFR/DPD structure [14].

Since filtering $c(n)$ may generate new peaks in $u_c(n)$, it is possible to repeat the CAF procedure for several iterations [24] and finally apply HC to definitely remove any remaining peak.

B. Conventional Joint CFR/DPD Structure

Compared with the traditional CFR method earlier, a joint CFR/DPD structure offers reduced running complexity if the CFR is implemented as a parametric model (MCFR) identical to the one used for the DPD since the CFR can simply be implemented as a correction of the DPD coefficients (see Section IV). The corresponding structure is shown in Fig. 2. The PAPR of the DPD output signal is reduced with an MCFR block.

The DPD and the MCFR share the same model structure Φ, respectively, with parameters β and α so that

$$\begin{aligned} c(n) &= \Phi_\alpha[u(n)] \\ x(n) &= \Phi_\beta[u(n)] \end{aligned} \quad (3)$$

where $u(n)$ is the system input signal or stimulus, $c(n)$ is the MCFR output, and $x(n)$ is the DPD output. Thus, the clipped predistorted signal $x_c(n)$ is

$$x_c(n) = x(n) - c(n) = \Phi_\theta[u(n)] \quad (4)$$

where $\theta = \beta - \alpha$.

Studies in [25] and [26] show that the GMP model structure has good linearization performance compared with other mathematical models. Moreover, since it is linear w.r.t. its parameters, the identification can be performed simply with least squares (LSs). In this article, we use the GMP for the joint CFR/DPD model structure, which can be written as

$$\begin{aligned} &\Phi_\theta[u(n)] \\ &= \sum_{k=0}^{\mathcal{K}_a-1}\sum_{l=0}^{\mathcal{L}_a-1} \theta_{a,kl}u(n-l)|u(n-l)|^k \\ &+ \sum_{k=1}^{\mathcal{K}_b}\sum_{l=0}^{\mathcal{L}_b-1}\sum_{m=1}^{\mathcal{M}_b} \theta_{b,klm}u(n-l)|u(n-l-m)|^k \\ &+ \sum_{k=1}^{\mathcal{K}_c}\sum_{l=0}^{\mathcal{L}_c-1}\sum_{m=1}^{\mathcal{M}_c} \theta_{c,klm}u(n-l)|u(n-l+m)|^k \end{aligned} \quad (5)$$

This article has been accepted for inclusion in a future issue of this journal. Content is final as presented, with the exception of pagination.

where k is the index for nonlinearity, and l and m are the indices for memory. The vector $\theta = [\theta_a, \theta_b, \theta_c]$ contains the complex coefficients for the signal and envelope, the signal and lagging envelope, and the signal and leading envelope, respectively. $\mathcal{K}_a$, $\mathcal{K}_b$, and $\mathcal{K}_c$ are the highest orders of nonlinearity. $\mathcal{L}_a$, $\mathcal{L}_b$, and $\mathcal{L}_c$ are the highest memory depths. $\mathcal{M}_b$ and $\mathcal{M}_c$ denote the longest lagging and leading delay tap lengths, respectively.

The MCFR coefficients α are estimated using the stimulus $u(n)$ and the reference correction signal $c_r(n)$, as shown in Fig. 2. This reference correction signal is obtained by applying a traditional CFR method, such as the CAF earlier, on the DPD output

$$c_r^{hc}(n) = \begin{cases} x(n)\left(1 - \dfrac{P}{|x(n)|}\right), & \text{if } |x(n)| \geq P \\ 0, & \text{otherwise} \end{cases} \tag{6}$$

and the conventional CAF with ideal rectangular window can be expressed in frequency domain as

$$\mathcal{F}\left\{c_r^{\text{caf}}\right\} = \begin{cases} \mathcal{F}\left\{c_r^{hc}\right\}(\omega), & \text{if } \omega \in \left[-\dfrac{B}{2}, \dfrac{B}{2}\right] \\ 0, & \text{otherwise} \end{cases} \tag{7}$$

where B is the bandwidth of the stimulus $u(n)$ and $\mathcal{F}\{\cdot\}$ represents discrete Fourier transform.

III. Proposed Joint CFR/DPD

The structure of the proposed CABF-based joint CFR/DPD is shown in Fig. 3, where $x_c(n)$ is the output signal of the joint CFR/DPD. The part with blue thick lines represents the signal transmission system of the test bench. Other parts are structures of model coefficient estimation, which can be computed without interrupting the signal transmission.

A. Model Identification

The identification of the joint CFR/DPD in Fig. 3 is based on indirect learning architecture (ILA). We estimate the values of α and β in an iterative procedure.

Inside each iteration, the DPD coefficients β are estimated before the CFR coefficients α. The first step is the identification of the postdistortion block using the PA input $x_c(n)$ and the signal $z(n)$, which is the PA output $y(n)$ divided by g, the desired loop gain. As different possible choices for g achieve about the same PA efficiency [27], we choose the small-signal gain in this article.

As mentioned earlier, one advantage of choosing a model structure derived from the Volterra series is that the model coefficients can be estimated by solving a linear problem. We can express the postdistortion using matrix notation for a block of N samples:

$$\boldsymbol{z_p} = \mathbf{Z}\boldsymbol{\beta} \tag{8}$$

where $\boldsymbol{z_p}=[z_p(1), \ldots, z_p(N)]^T$, $\boldsymbol{z}=[z(1), \ldots, z(N)]^T$, $\mathbf{Z}$ is $N \times R$ matrix containing basis functions of $\boldsymbol{z}$, and $R = \mathcal{K}_a\mathcal{L}_a + \mathcal{K}_b\mathcal{L}_b\mathcal{M}_b + \mathcal{K}_c\mathcal{L}_c\mathcal{M}_c$ is the total number of coefficients. The LS estimation of $\boldsymbol{\beta}$ is found by

$$\hat{\boldsymbol{\beta}} = [\mathbf{Z}^H\mathbf{Z}]^{-1}\mathbf{Z}^H\boldsymbol{x_c} \tag{9}$$

which minimizes the cost function

$$C = \sum_{n=1}^{N} |z_p(n) - x_c(n)|^2. \tag{10}$$

The identified postdistortion is then applied upstream of the PA as the DPD.

With the current estimate $\hat{\boldsymbol{\beta}}$, the CFR model coefficients $\boldsymbol{\alpha}$ can be estimated to reduce the PAPR at the DPD output by

$$\hat{\boldsymbol{\alpha}} = [\mathbf{U}^H\mathbf{U}]^{-1}\mathbf{U}^H\boldsymbol{c_r} \tag{11}$$

where $\boldsymbol{U}$ is the basis function matrix of $\boldsymbol{u}$, and $\boldsymbol{c_r}$ is the vector of reference correction signal.

The initial value of $\boldsymbol{\alpha}$ is an array of 0. The initial value of $\boldsymbol{\beta}$ is $[1, 0, \ldots, 0]$. Thus, at the first iteration, $\boldsymbol{x_c} = \boldsymbol{u}$. We repeat four iterations in this article for convergence.

Since α is estimated according to $\boldsymbol{u}$ and $\boldsymbol{c_r}$, the generation method of $\boldsymbol{c_r}$ has a great impact on the system performance. Simulations previously showed that the CABF approach could outperform the conventional CAF approach in generating $\boldsymbol{c_r}$ with a single-carrier stimulus [23].

B. CABF-Based Joint CFR/DPD With Single-Carrier Stimulus

The reference correction signal is determined using a clipped version of the DPD output to limit the PA input under a certain threshold. The maximum PA input peak power P_{PAinPeak} is constrained by its corresponding output power being the edge of the PA saturation zone, as shown in Fig. 4. In the following, we denote the clipping threshold of the CFR with $P = P_{\text{PAinPeak}}$.

In this section, we consider a stimulus with only one carrier. Since the chosen DPD model is based on Volterra series, the predistorted signal $x(n)$ contains the nonlinearities brought by $|u(n)|^k$ according to (3) and (5). Hence, the bandwidth B is not appropriate for $x(n)$. We decompose $x(n)$ into signals of different nonlinearity orders as

$$x(n) = \sum_{k \in \mathcal{K}} g_k(n) \tag{12}$$

where

$$\begin{aligned} g_k(n) = & \sum_{l=0}^{\mathcal{L}_a-1} \beta_{a,kl} u(n-l)|u(n-l)|^{k-1} \\ & + \sum_{l=0}^{\mathcal{L}_b-1} \sum_{m=1}^{\mathcal{M}_b} \beta_{b,klm} u(n-l)|u(n-l-m)|^{k-1} \\ & + \sum_{l=0}^{\mathcal{L}_c-1} \sum_{m=1}^{\mathcal{M}_c} \beta_{c,klm} u(n-l)|u(n-l+m)|^{k-1} \end{aligned} \tag{13}$$

is the signal with nonlinearity order k. Since $u(n)$ is limited in $[-(B)/(2), (B)/(2)]$, the spectrum of $g_k(n)$ occupies the band $[-k(B)/(2), k(B)/(2)]$. In order to keep the nonlinearity information in $x(n)$, we clip and filter each $g_k(n)$ separately within corresponding bands.

This article has been accepted for inclusion in a future issue of this journal. Content is final as presented, with the exception of pagination.

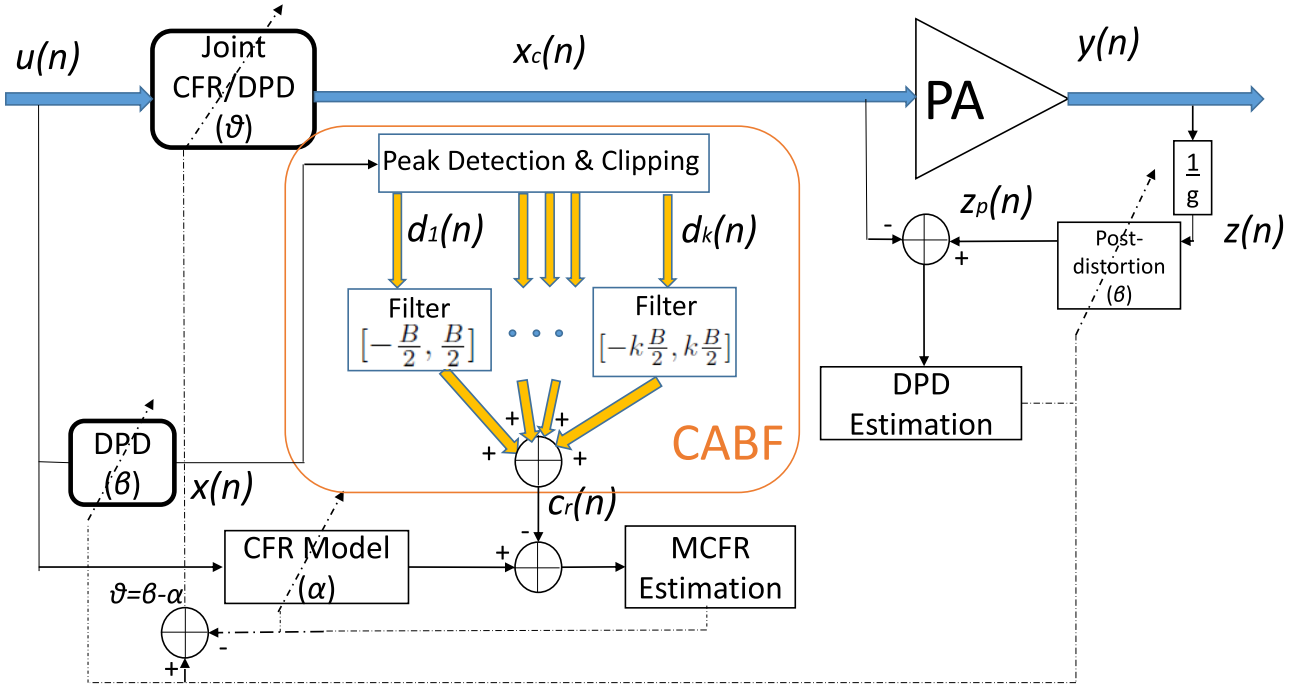

Fig. 3. Proposed joint CFR/DPD structure.

As shown in Fig. 3, first we detect the peaks of $x(n)$ to get the clipped signal $d_k(n)$ corresponding to each $g_k(n)$

$$d_k(n) = \begin{cases} g_k(n)\left(1 - \dfrac{P}{|x(n)|}\right), & \text{if } |x(n)| \geq P \\ 0, & \text{otherwise.} \end{cases} \quad (14)$$

Then, $d_k(n)$ is filtered according to its nonlinearity order k:

$$\mathcal{F}\{d_k^{\text{caf}}\} = \begin{cases} \mathcal{F}\{d_k\}(\omega) \cdot W_k(\omega), & \text{if } \omega \in \left[-k\dfrac{B}{2}, k\dfrac{B}{2}\right] \\ 0, & \text{otherwise} \end{cases} \quad (15)$$

where $W_k(\omega)$ is a window centered at frequency 0 with width $[-k(B)/(2), k(B)/(2)]$. The window length is equal to the number of samples of $\mathcal{F}\{d_k\}(\omega)$. Since $g_k(n)$ $(k > 1)$ occupies a larger band than $g_1(n)$, filtering $d_k(n)$ increases the errors in bands $[-k(B)/(2), -(B)/(2)]$ and $[(B)/(2), k(B)/(2)]$, which deteriorates the ACPR. Hence, we propose to apply nonrectangular windows $W_k(\omega)$ to shape the filters and to smooth out the error.

As can be done with conventional CAF, we apply HC on the final signal to ensure no peak exceeding P after repeating the clipping and filtering steps. The reference correction signal is finally computed as

$$c_r^{\text{cabf}}(n) = \sum_{k \in \mathcal{K}} d_k^{\text{caf}}(n). \quad (16)$$

C. Choice of Windows

The choice of windows $W_k(\omega)$ has an impact on linearization performance. To compare different windows based on their intrinsic performance without any influence of the MCFR parametric model, we do not estimate the MCFR coefficients but simply pass the clipped reference signal

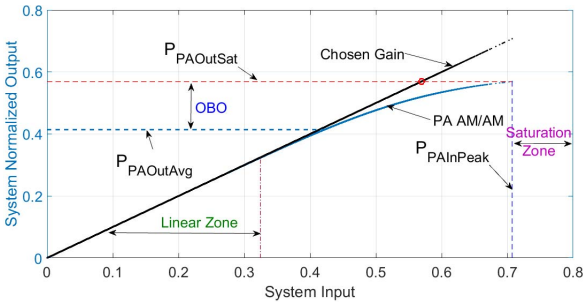

Fig. 4. PA output signal versus PA input signal.

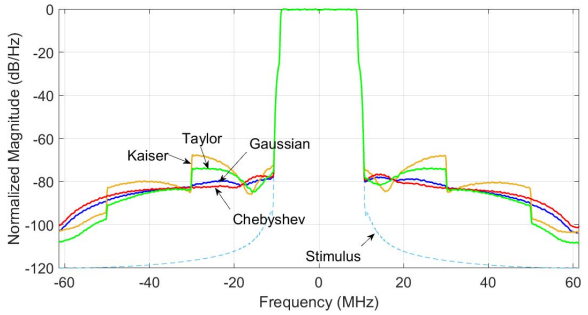

Fig. 5. Test of different windows for CABF.

$x_{cr}(n) = x(n) - c_r^{\text{cabf}}(n)$ to the PA and evaluate the corresponding PA output spectrum.

In order to test the performance of different windows, a Wiener model PA with 1-dB compression output power at 25 dBm is used for the simulation on MATLAB. A 20-MHz LTE signal with 90 000 samples is used as a stimulus. Its PAPR at the 10^{-4} probability level is 8 dB. The spectra of the PA output with 8-dB backoff applied are shown in Fig. 5. The ACPR values are listed in Table I. As a reference, the ACPR value results for the clipped reference signal

This article has been accepted for inclusion in a future issue of this journal. Content is final as presented, with the exception of pagination.

TABLE I
IMPACTS ON PA LINEARITY WITH DIFFERENT WINDOWS FOR CABF

Window Name	ACPR (dBc)			
	L1	U1	L2	U2
Hann	-76.3	-75.2	-83.5	-84.7
Gaussian	-76.7	-75.9	-82.1	-83.0
Hamming	-75.4	-74.4	-82.8	-83.7
Kaiser	-71.3	-71.3	-78.6	-79.0
Blackman	-77.1	-76.2	-82.5	-83.5
Bohman	-77.3	-76.3	-82.4	-83.3
Bartlett	-74.7	-74.0	-81.3	-82.3
Chebyshev	-77.3	-76.6	-81.4	-82.1
Taylor	-74.0	-73.4	-83.2	-83.6

L(U)1(2): First(Second) lower(upper) adjacent channel

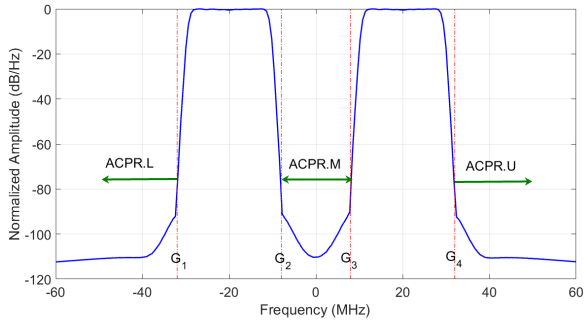

Fig. 6. Notions of bands in case of multicarrier stimulus.

obtained with conventional CAF are in dBc (−71.5 and −71.1) for L1/U1 and (−72.0 and −72.3) for L2/U2. The Chebyshev window with 100 dB of sidelobe attenuation can reach the best first channel ACPR values (ACPR.L1 and ACPR.U1) and will be used in this article.

In Section III-D, we consider the case where the stimulus has multiple carriers.

D. CABF-Based Joint CFR/DPD With Multicarrier Stimulus

When using a single-carrier CABF with the stimulus consisting of multiple carriers, the out-of-band distortion brought by clipping will not be filtered out between channels. Taking the example of a two-carrier signal, as shown in Fig. 6, the ACPR needs to be improved not only in lower (ACPR.L) and upper channels (ACPR.U) but also the middle channel (ACPR.M), whose frequency band is $[G_2, G_3]$.

We can reduce the values of ACPR.L and ACPR.U using the filter (15) in Section III-C. However, in order to filter the middle channel, the windows need to be adapted in the band $[G_2, G_3]$.

A T-carrier stimulus occupies T frequency bands centered at f_c^i, where $i = 1, \ldots, T$, of widths B_i and limits $[G_{2i-1}, G_{2i}]$. The distortion on side channels (L and U) and middle channel (M) are treated separately.

First, for the distortion on side channels, we take the signal as a single carrier of bandwidth $B_0 = G_{2T} - G_1$ and use the method of (15) with the global window $W_k^0(\omega)$ defined on $[-k(B_0)/(2), k(B_0)/(2)]$.

Second, for the distortion on middle channels $[G_{2i}, G_{2i+1}]$ where $i = 1, \ldots, T-1$, we can first treat them individually as the side channels of each carrier. For the carrier at f_c^i, we create a local window $W_k^i(\omega)$ in band $[f_c^i - k(B_i)/(2), f_c^i + k(B_i)/(2)]$. When the nonlinearity order k is high enough, the windows for the different carriers may overlap with each other. We take the maximum value among them $\max_i(W_k^i(\omega))$ at each overlapped frequency ω. Thus, the inner window $\Omega_k(\omega)$ in the frequency $[G_1, G_{2T}]$ is obtained by combining the $W_k^i(\omega)$ into

$$\Omega_k(\omega) = \max_i \left(W_k^i(\omega)\right), \quad \omega \in [G_1, G_{2T}]. \tag{17}$$

We apply this inner window only on the middle channels

$$\mathcal{F}\{d_k^{\text{caf}}\} = \begin{cases} \mathcal{F}\{d_k\}(\omega) \cdot W_k^0(\omega), & \text{if } \omega \in \mathcal{O} \\ \mathcal{F}\{d_k\}(\omega) \cdot \Omega_k(\omega), & \text{if } \omega \in \mathcal{U} \\ 0, & \text{otherwise} \end{cases} \tag{18}$$

where $\mathcal{U}$ is the union of the middle channels, and $\mathcal{O}$ is the complementary such that $\mathcal{U} \cup \mathcal{O} = [-k(B_0)/(2), k(B_0)/(2)]$

$$\begin{aligned} \mathcal{U} &= [G_2, G_3] \cup \cdots \cup [G_{2T-2}, G_{2T-1}] \\ \mathcal{O} &= \left[-k\frac{B}{2}, G_2\right] \cup [G_3, G_4] \cup \cdots \cup \left[G_{2T-1}, k\frac{B}{2}\right]. \end{aligned} \tag{19}$$

The reference correction signal is then obtained by (16).

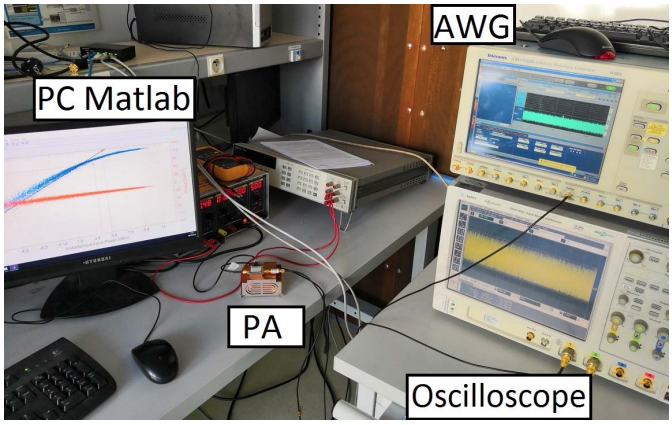

Fig. 7. Test bench for experimental implementation.

IV. EXPERIMENTAL RESULTS

A. Test Bench

The test bench is shown in Fig. 7. Two PAs are used as a device under test (DUT) in this section: an HMC409LP4E PA working in 3.3–3.8 GHz for the single-carrier test and a TA020-060-30-27 PA working in 2–6 GHz for the multiple-carrier test.

We generate the modulated signal in the PC workstation and feed it to the PA through an arbitrary waveform generator (AWG) with 10-GHz sampling frequency.

The PA output signal is captured by an oscilloscope and is fed back to the PC workstation for postdistortion processing. The input and output baseband signals are synchronized in time after downsampling to 120 MHz for the single-carrier stimulus and 600 MHz for the multicarrier stimulus to be used by the identification algorithm.

This article has been accepted for inclusion in a future issue of this journal. Content is final as presented, with the exception of pagination.

TABLE II
NUMBER OF FLOPS FOR OPERATIONS

Operation	FLOPs	Operation	FLOPs
Real Addition	1	Real Multiplication	1
Real Division	4	Complex Addition	2
Complex Multiplication	6	Complex-Real Multiplication	2
Square-root	6~8		

We feed a segment of 90 000 samples signal to the AWG for transmission. The coefficients of the proposed joint CFR/DPD are estimated with 40 000 samples in each iteration. The model identification stops after its linearization performance converges. In the implementations of this article, we keep updating the model coefficients for four iterations. The performance is evaluated with the signal of 90 000 samples.

B. Running Complexity

Since the identification of models is required only when the input signal or the PA behavior is changed, here we consider only running complexity [25]. For the conventional CAF-DPD method, we calculate the complexities of the CAF and the DPD separately, and their sum is considered as the total complexity of the system. For the joint CFR/DPD model, there is only one model that has the same structure as the DPD model. Thus, its complexity should be equal to the complexity of the DPD. The only difference that the proposed method exhibits with respect to conventional joint CFR/DPD is regarding model coefficient estimation. Therefore, their running complexities are identical.

We estimate the complexity of each method by the number of floating-point operations (FLOPs). Table II gives the number of FLOPs of each operation according to [25]. Since different algorithms are available for the square-root operation, the number of FLOPs is around 6–8. We take an average of 7 FLOPs in this article.

1) Joint CFR/DPD Complexity Estimation: The joint CFR/DPD is implemented with a GMP model in this article. According to [25], the running complexity of a GMP model for an N-sample signal can be expressed as

$$F_{\text{GMP}} = (8R - 2)N \tag{20}$$

where R is the number of model coefficients.

2) CAF Complexity Estimation: We clip and filter the signal iteratively using the CAF approach. By detecting the peaks, one complex modulus is computed for each sample. In order to reduce the number of processed samples, the peak windowing technique is taken in place of a low-pass filter. A Gaussian window is applied on S samples centered at the clipped peak. Two complex subtractions (four FLOPs) on each sample are implemented before and after filtering. The number of peaks detected decreases as long as the number of CAF iteration increases. If we denote the average number of peaks per iteration as $\bar{N_p}$, the number of FLOPs for an N-sample signal at each iteration is $14N + \bar{N_p}(6 + 2S)$.

If there are still N'_p peaks remained after I_m iterations for CAF, we hard clip them. The total number of FLOPs is then

$$F_{\text{CAF}} = I_m[14N + \bar{N_p}(6 + 2S)] + \left(10N + 6N'_p\right). \tag{21}$$

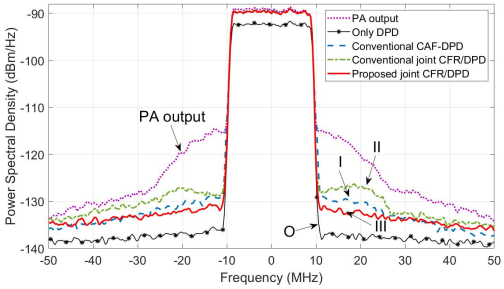

O: Only DPD without CFR; I: Conventional CAF-DPD method; II: Conventional joint CFR/DPD method; III: Proposed joint CFR/DPD method

Fig. 8. PA output spectra for various system configurations: without DPD, with DPD only, and with DPD and CFR using methods I, II, and III for single-carrier 20-MHz LTE.

TABLE III
COMPARISON OF DIFFERENT METHODS WITH SINGLE-CARRIER 20-MHz LTE STIMULUS

		O	I	II	III
P_{out} (dBm)		24.2	26.8	26.6	26.6
I_{supply} (A)		0.63	0.68	0.68	0.68
PAE (%)		8.4	14.1	13.4	13.4
ACPR (dBc)	L1	-45.0	-40.9	-38.6	-42.7
	U1	-45.7	-41.0	-38.4	-43.3
	L2	-46.3	-45.0	-42.8	-45.0
	U2	-46.8	-46.0	-44.3	-45.8
EVM (%)		2.4	3.6	4.5	4.7
Complexity (flops)		$1.49e^7$	$2.87e^7$	$1.49e^7$	$1.49e^7$

O: Only DPD without CFR
I: Conventional CAF-DPD method
II: Conventional joint CFR/DPD method
III: Proposed joint CFR/DPD method

In this article, we set the Gaussian window width $S = 100$ and CAF iteration number $I_m = 10$.

C. Measurement Result With Single-Carrier Stimulus

In this section, we use as stimulus a 20-MHz LTE signal with PAPR equal to 8 dB at 3.5-GHz carrier frequency. The DUT is an HMC409LP4E PA fabricated by Analog Devices, Inc., Norwood, MA, USA. Its nominal gain at 3.5-GHz frequency is 31 dB, and the output power at 1-dB compression point is 32.5 dBm. The supply voltage is 5 V. The proposed joint CFR/DPD is tested on the test bench and is compared with the conventional CAF-DPD method and the conventional joint CFR/DPD method.

With the PA input and output signals, the optimal DPD model structure determined by the algorithm in [21] is

$$\begin{aligned} \mathcal{K}_a &= 2, \quad \mathcal{L}_a = 4 \\ \mathcal{K}_b &= 1, \quad \mathcal{L}_b = 1, \ \mathcal{M}_b = 1 \\ \mathcal{K}_c &= 6, \quad \mathcal{L}_c = 2, \ \mathcal{M}_c = 1. \end{aligned} \tag{22}$$

For the sake of simplicity, we use the same DPD model structure for the joint CFR/DPD model.

The PA output spectra linearized with different methods are shown in Fig. 8. The pink dotted curve is the PA output without DPD linearization. The black star curve stands for the PA output linearized by only DPD (method O). The blue dashed curve

This article has been accepted for inclusion in a future issue of this journal. Content is final as presented, with the exception of pagination.

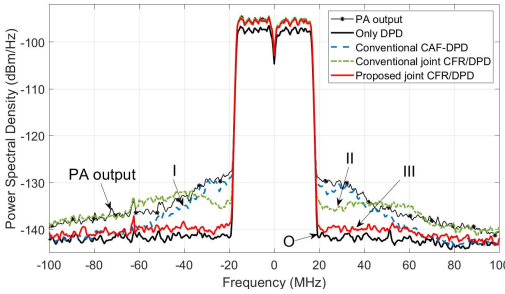

O: Only DPD without CFR; I: Conventional CAF-DPD method; II: Conventional joint CFR/DPD method; III: Proposed joint CFR/DPD method

Fig. 9. PA output spectra for various system configurations: without DPD, with DPD only, and with DPD and CFR using methods I, II, and III for single-carrier 40-MHz WLAN signal.

represents the conventional CAF-DPD method (method I). The green dashed-dotted curve represents the conventional CFR/DPD method (method II). The red curve represents the proposed CABF-based CFR/DPD method (method III).

The corresponding ACPR, EVM values, complexities, the currents of supply (I_{supply}), and PA power-added efficiencies (PAE) are given in Table III. The complexities are estimated at $N = 90\,000$ samples.

The EVM values of all approaches are less than 5%. The result of method O (only DPD without CFR) is given as a reference.

The operating point of the method O is limited by the PAPR of the stimulus. Compared with the method O, the other methods with CFR, which reduces the PAPR of around 2.5 dB, can improve the PAE from 8.4% to at least 13.4%. These results confirm the benefit of the CFR techniques on power efficiency improvement.

Compared with the method I, the method II has lower complexity but worse linearization performance. Compared with method I and II, our proposed joint CFR/DPD (method III) has overall better ACPR values and complexity. We save 48% of the complexity from the conventional CAF-DPD method. The ACPR values of the proposed joint CFR/DPD on the first adjacent channels have an advantage beyond the conventional joint CFR/DPD of up to 5 dB.

We also test these approaches using a 40-MHz wireless local area network (WLAN) signal as the stimulus. The PAPR of the stimulus is 12 dB. The optimal DPD model structure becomes

$$\begin{aligned} &\mathcal{K}_a = 1, \quad \mathcal{L}_a = 11 \\ &\mathcal{K}_b = 3, \quad \mathcal{L}_b = 2, \ \mathcal{M}_b = 1 \\ &\mathcal{K}_c = 8, \quad \mathcal{L}_c = 2, \ \mathcal{M}_c = 1. \end{aligned} \tag{23}$$

The PA output spectra obtained for different CFR and DPD approaches are shown in Fig. 9. The numerical results are listed in Table IV.

The PA output power is increased by 2 dB with the combined CFR and DPD methods (methods I–III), which renders an improvement of 56% on the PA efficiency. Our proposed method (method III) has a very good performance on PA linearization and complexity compared with the methods I and II. The EVM value is kept under 5%.

These experimental results validate the robustness of the proposed CABF-based joint CFR/DPD. Since one aim of CFR is to increase the PA power efficiency by pushing its operating point toward the saturation zone, the PA linearity should deteriorate. At the same operating point, our proposed method reaches better ACPR values compared with the conventional methods. In other words, it provides a larger range of operating point choices since it gives a larger margin on ACPR.

The performance of the proposed joint CFR/DPD is also evaluated with different models (22) and (23). The PA output spectra of these tests are shown in Figs. 10 and 11 using the LTE and WLAN signals, respectively. The corresponding ACPR and EVM values and complexities are listed in Table V.

When using the LTE signal as the stimulus, model (23) keeps a good linearization performance. The complexity of

TABLE IV

COMPARISON OF DIFFERENT METHODS WITH SINGLE-CARRIER 40-MHz WLAN STIMULUS

		O	I	II	III
P_{out} (dBm)		20.5	22.6	22.7	22.4
I_{supply} (A)		0.63	0.63	0.63	0.63
PAE (%)		3.6	5.6	5.9	5.5
ACPR (dBc)	L1	-44.2	-35.9	-37.5	-43.3
	U1	-44.6	-35.8	-39.0	-43.4
	L2	-44.8	-42.1	-42.1	-44.5
	U2	-45.9	-43.3	-44.1	-45.6
EVM (%)		3.5	2.2	4.6	2.4
Complexity (flops)		$2.34e^7$	$7.29e^7$	$2.34e^7$	$2.34e^7$

O: Only DPD without CFR
I: Conventional CAF-DPD method
II: Conventional joint CFR/DPD method
III: Proposed joint CFR/DPD method

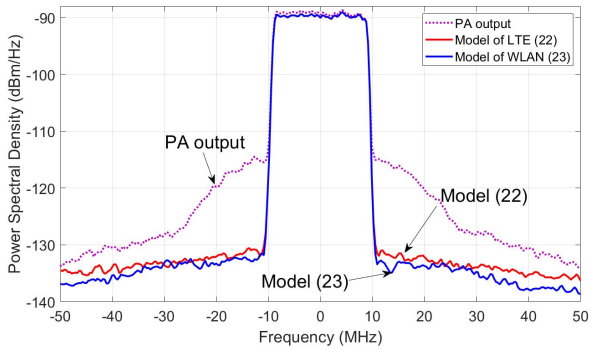

Fig. 10. PA output spectra with proposed joint CFR/DPD method using different models for single-carrier 20-MHz LTE signal.

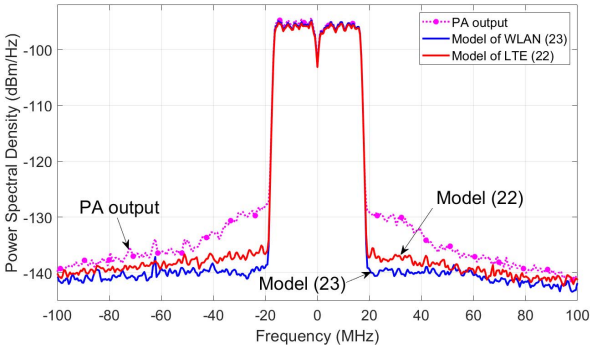

Fig. 11. PA output spectra with proposed joint CFR/DPD method using different models for single-carrier 40-MHz WLAN signal.

This article has been accepted for inclusion in a future issue of this journal. Content is final as presented, with the exception of pagination.

TABLE V
COMPARISON OF DIFFERENT MODELS

Signal		LTE		WLAN	
Model		(22)	(23)	(22)	(23)
ACPR (dBc)	L1	-42.7	-42.9	-40.7	-43.3
	U1	-43.3	-43.8	-41.4	-43.4
	L2	-45.0	-46.0	-42.8	-44.5
	U2	-45.8	-47.4	-44.1	-45.6
EVM (%)		4.7	3.6	3.0	2.4
Complexity (flops)		$1.49e^7$	$2.34e^7$	$1.49e^7$	$2.34e^7$

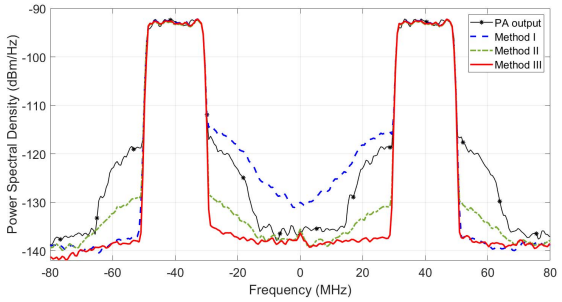

I: Conventional CAF-DPD method; II: Conventional joint CFR/DPD method; III: Proposed joint CFR/DPD method

Fig. 12. PA output spectra for various system configurations: without DPD, and with DPD and CFR using methods I, II, and III for two-carrier 20-MHz LTE.

(23) is higher, but comparing with the conventional CFR-DPD method in Table III, we can still save 23% of complexity. When using the WLAN signal as the stimulus, model (22) degrades over 2 dB on ACPR with much lower complexity.

D. Measurement Result With Two-Carrier Stimulus

We test the proposed multicarrier CABF-based joint CFR/DPD in this section. The DUT in the test bench is a TA020-060-30-27 PA fabricated by Transcom, Inc., Tainan, Taiwan. Its nominal gain is 30 dB, and the output power at 1-dB gain compression is 27 dBm. A two-carrier LTE signal is used as the stimulus with 10-dB PAPR. The lower band carrier frequency is 2100 MHz, and the upper band carrier frequency is 2180 MHz. These two components have both 20-MHz bandwidth. We use a GMP model for the DPD with $\mathcal{K}_a = 5$, $\mathcal{L}_a = 2$, and $\mathcal{K}_b = \mathcal{K}_c = 0$, which corresponds to an MP model.

The PA output spectra linearized with different methods are shown in Fig. 12. The black star curve gives the PA output without DPD linearization. The blue dashed curve shows the performance of the conventional CAF-DPD method (method I). The green dashed-dotted curve results from the conventional CFR/DPD method (method II). The red curve is the spectrum of the proposed CABF-based CFR/DPD method (method III).

The corresponding ACPR, EVM values, and complexities are given in Table VI. Since the advantage of PA efficiency of applying CFR has been addressed, here we compare only the results of the methods with CFR at the same PA operating point. For ACPR values, we estimate band L (from -70 to -50 MHz) and M.L (from -30 to -10 MHz) for the lower band carrier, and band M.U (from 10 to 30 MHz) and U (from 50 to 70 MHz) for the upper band carrier. The complexities are estimated at $N = 90\,000$ samples.

TABLE VI
COMPARISON OF DIFFERENT METHODS WITH TWO-CARRIER STIMULUS

		I	II	III
ACPR (dBc)	L	-45.0	-39.2	-44.9
	M.L	-26.2	-39.6	-43.1
	M.U	-26.2	-40.1	-43.9
	U	-44.9	-40.8	-44.4
EVM (%)		3.2	6.8	3.7
Complexity (flops)		$2.56e^7$	$7.02e^6$	$7.02e^6$

I: Conventional CAF-DPD method
II: Conventional joint CFR/DPD method
III: Proposed joint CFR/DPD method

The EVM value of our proposed method is kept at less than 4%. By using the joint CFR/DPD structure, the methods II and III save 72% of the complexity from the conventional CAF-DPD method. Compared with the method II, our proposed CABF-based method exhibits better ACPR performance, and the improvements in the middle band (M.L/U) and lower/upper band (L/U) are around 4 dB.

The comparison against the conventional methods in Table VI shows that our proposed CABF-based joint CFR/DPD achieves good performance on both the sidebands and the middle band with lower complexity.

V. CONCLUSION

This article explores a CABF-based joint CFR/DPD approach when the system input signal can have multiple carriers. Experimental results with two different PAs show that the proposed approach takes full advantage of the joint CFR/DPD paradigm in terms of complexity reduction while simultaneously providing better linearization performances than conventional joint CFR/DPD methods in both single-carrier and multicarrier cases. Concerning the choice of windows for the bank filtering, Chebychev windows are suggested since they give the most relevant performance in terms of ACPR.

REFERENCES

[1] L. Guan and A. Zhu, "Green communications: Digital predistortion for wideband RF power amplifiers," *IEEE Microw. Mag.*, vol. 15, no. 7, pp. 84–99, Nov. 2014.
[2] F. H. Raab, "Efficiency of Doherty RF power-amplifier systems," *IEEE Trans. Broadcast.*, vol. BC-33, no. 3, pp. 77–83, Sep. 1987.
[3] A. Katz, J. Wood, and D. Chokola, "The evolution of PA linearization: From classic feedforward and feedback through analog and digital predistortion," *IEEE Microw. Mag.*, vol. 17, no. 2, pp. 32–40, Feb. 2016.
[4] J. Kim and K. Konstantinou, "Digital predistortion of wideband signals based on power amplifier model with memory," *Electron. Lett.*, vol. 37, no. 23, pp. 1417–1418, Nov. 2001.
[5] L. Ding *et al.*, "A robust digital baseband predistorter constructed using memory polynomials," *IEEE Trans. Commun.*, vol. 52, no. 1, pp. 159–165, Jan. 2004.
[6] D. R. Morgan, Z. Ma, J. Kim, M. G. Zierdt, and J. Pastalan, "A generalized memory polynomial model for digital predistortion of RF power amplifiers," *IEEE Trans. Signal Process.*, vol. 54, no. 10, pp. 3852–3860, Oct. 2006.
[7] A. Zhu, J. C. Pedro, and T. J. Brazil, "Dynamic deviation reduction-based Volterra behavioral modeling of RF power amplifiers," *IEEE Trans. Microw. Theory Techn.*, vol. 54, no. 12, pp. 4323–4332, Dec. 2006.

This article has been accepted for inclusion in a future issue of this journal. Content is final as presented, with the exception of pagination.

[8] F. Mkadem, M. C. Fares, S. Boumaiza, and J. Wood, "Complexity-reduced Volterra series model for power amplifier digital predistortion," *Analog Integr. Circuits Signal Process.*, vol. 79, no. 2, pp. 331–343, Feb. 2014.

[9] A. Zhu, "Decomposed vector rotation-based behavioral modeling for digital predistortion of RF power amplifiers," *IEEE Trans. Microw. Theory Techn.*, vol. 63, no. 2, pp. 737–744, Feb. 2015.

[10] T. Liu, S. Boumaiza, and F. M. Ghannouchi, "Augmented Hammerstein predistorter for linearization of broad-band wireless transmitters," *IEEE Trans. Microw. Theory Techn.*, vol. 54, no. 4, pp. 1340–1349, Jun. 2006.

[11] S. Chen, "An efficient predistorter design for compensating nonlinear memory high power amplifiers," *IEEE Trans. Broadcast.*, vol. 57, no. 4, pp. 856–865, Dec. 2011.

[12] S. Wang, M. A. Hussein, O. Venard, and G. Baudoin, "Optimal sizing of two-stage cascaded sparse memory polynomial model for high power amplifiers linearization," *IEEE Trans. Microw. Theory Techn.*, vol. 66, no. 9, pp. 3958–3965, Sep. 2018.

[13] J. Wood, *Behavioral Modeling and Linearization of RF Power Amplifiers* (Artech House Microwave Library). Norwood, MA, USA: Artech House, 2014.

[14] R. N. Braithwaite, "A combined approach to digital predistortion and crest factor reduction for the linearization of an RF power amplifier," *IEEE Trans. Microw. Theory Techn.*, vol. 61, no. 1, pp. 291–302, Jan. 2013.

[15] A. Mbaye, G. Baudoin, A. Gouba, Y. Louet, and M. Villegas, "Combining crest factor reduction and digital predistortion with automatic determination of the necessary crest factor reduction gain," in *Proc. 44th Eur. Microw. Conf.*, Oct. 2014, pp. 837–840.

[16] X. Chen, W. Chen, F. Huang, F. M. Ghannouchi, Z. Feng, and Y. Liu, "Systematic crest factor reduction and efficiency enhancement of dual-band power amplifier based transmitters," *IEEE Trans. Broadcast.*, vol. 63, no. 1, pp. 111–122, Mar. 2017.

[17] S. Wang, M. Roger, and C. Lelandais-Perrault, "Impacts of crest factor reduction and digital predistortion on linearity and power efficiency of power amplifiers," *IEEE Trans. Circuits Syst. II, Exp. Briefs*, vol. 66, no. 3, pp. 407–411, Mar. 2019.

[18] H. Enzinger, K. Freiberger, and C. Vogel, "Competitive linearity for envelope tracking: Dual-band crest factor reduction and 2D-vector-switched digital predistortion," *IEEE Microw. Mag.*, vol. 19, no. 1, pp. 69–77, Jan./Feb. 2018.

[19] M. V. Amiri, M. Helaoui, N. Boulejfen, and F. M. Ghannouchi, "Optimized spectrum constrained crest factor reduction technique using polynomials," *IEEE Trans. Commun.*, vol. 63, no. 7, pp. 2555–2564, Jul. 2015.

[20] A. Mämmelä and A. Anttonen, "Why will computing power need particular attention in future wireless devices?" *IEEE Circuits Syst. Mag.*, vol. 17, no. 1, pp. 12–26, 1st Quart., 2017.

[21] S. Wang, M. A. Hussein, O. Venard, and G. Baudoin, "A novel algorithm for determining the structure of digital predistortion models," *IEEE Trans. Veh. Technol.*, vol. 67, no. 8, pp. 7326–7340, Aug. 2018.

[22] M. A. Hussein, V. A. Bohara, and O. Venard, "On the system level convergence of ILA and DLA for digital predistortion," in *Proc. Int. Symp. Wireless Commun. Syst. (ISWCS)*, Aug. 2012, pp. 870–874.

[23] S. Wang, M. Roger, and C. Lelandais-Perrault, "Clipping-and-bank-filtering technique in joint crest factor reduction and digital predistortion for power amplifiers," in *Proc. Asia–Pacific Microw. Conf. (APMC)*, Nov. 2018, pp. 768–770.

[24] K. Anoh, C. Tanriover, and B. Adebisi, "On the optimization of iterative clipping and filtering for PAPR reduction in OFDM systems," *IEEE Access*, vol. 5, pp. 12004–12013, 2017.

[25] A. S. Tehrani, H. Cao, T. Eriksson, M. Isaksson, and C. Fager, "A comparative analysis of the complexity/accuracy tradeoff in power amplifier behavioral models," *IEEE Trans. Microw. Theory Techn.*, vol. 58, no. 6, pp. 1510–1520, Jun. 2010.

[26] C. Kantana, O. Venard, and G. Baudoin, "Comparison of GMP and DVR models," in *Proc. Int. Workshop Integr. Nonlinear Microw. Millimetre-Wave Circuits (INMMIC)*, Jul. 2018, pp. 1–3.

[27] S. Wang, M. A. Hussein, O. Venard, and G. Baudoin, "Impact of the normalization gain of digital predistortion on linearization performance and power added efficiency of the linearized power amplifier," in *Proc. 12th Eur. Microw. Integr. Circuits Conf. (EuMIC)*, Oct. 2017, pp. 310–313.

Siqi Wang received the B.S. degree from the Huazhong University of Science and Technology, Wuhan, China, in 2012, the M.S. degree from the University of Paris-Sud, Orsay, France, in 2014, and the Ph.D. degree from the University of Paris-Est Marne-la-Vallée, Champs-sur-Marne, France, in 2018.

He is currently a Post-Doctoral Fellow with the GeePs, CentraleSupélec, Gif-sur-Yvette, France. His research interests include wireless communications, digital predistortion, and energy efficiency optimization for wireless communication systems.

Morgan Roger (M'18) received the Engineering degree with a focus on mechanics, electrical engineering and electronics from the Ecole Spéciale des Travaux Publics, Paris, France, in 2002, and the Ph.D. degree in signal processing from the University of Paris-Sud, Orsay, France, in 2007.

In 2002, he joined the Department of Electronic Systems, CentraleSupélec, Gif-sur-Yvette, France, where he is currently an Associate Professor with the GeePs. His current research interests include data converters and signal processing methods for electronic systems with an emphasis on power amplifier linearization.

Julien Sarrazin (S'05–M'12) received the master's degree in engineering and the Ph.D. degree from the University of Nantes, Nantes, France, in 2005 and 2008, respectively.

From 2009 and 2010, he was with the B. K. Birla Institute of Technology of Pilani, Pilani, India, where he was in charge of telecommunication-related teaching. From 2011 to 2012, he was a Research Engineer with Télécom Paris, Paris, France. Since 2012, he has been an Associate Professor with Sorbonne Université (formerly University of Pierre and Marie Curie), Paris, where he is currently with the Electronics and Electromagnetism Lab (L2E), where he is involved in the field of spatial data focusing and localization. His research interests include antenna design and channel modeling for body area networks. He has published over 90 technical journals, patents, book chapters, and conference articles.

Dr. Sarrazin is a reviewer.

Caroline Lelandais-Perrault received the Diploma degree from the École supérieure d'électricité, Gif-sur-Yvette, France, in 1995, and the Ph.D. degree from the University of Paris-Sud, Orsay, France, in 2006.

She worked six years as a Development Engineer and a Project Manager with IN-SNEC (Zodiac Data Systems), Plaisir, France, a company specialized in telemetry equipment for satellites and Ariane rocket. In 2001, she joined the Electronic System Department, Supélec. She is currently an Associate Professor with the GeePs (UMR CNRS 8507), Department of Electronic Systems, CentraleSupélec, University of Paris-Saclay, Saint-Aubin, France. Her current research interests include wideband and versatile, high-resolution analog-to-digital conversion, and calibration techniques of those systems.